Colloid Polym Sci 273:1080–1087 (1995)

ORIGINAL CONTRIBUTION

H. Hirata
S. Aoki
K. Taga
H. Okabayashi
T. Yoshida
T. Kawakatsu

Phase diagram and phase structure of the sodium di-*n*-pentyl phosphate-water system. ^{1}H pulsed-gradient NMR self-diffusion, ^{31}P NMR and x-ray diffraction studies

Received: 20 April 1995
Accepted: 19 July 1995

H. Hirata · S. Aoki · K. Taga
Dr. H. Okabayashi (✉) · T. Yoshida
Department of Applied Chemistry
Nagoya Institute of Technology
Gokiso-cho, Showa-ku
Nagoya 466, Japan

T. Kawakatsu
Department of Physics
Tokyo Metropolitan University
Hachioji Tokyo 19-03, Japan

Abstract Sodium di-*n*-pentylphos phate (DPP) has been synthesized, and the phase diagram of the DPP-water system consisting of five regions (I, II, III, IV, and V) has been determined. The phase structure has been investigated by ^{1}H pulsed-gradient NMR self-diffusion, ^{31}P NMR and x-ray low angle diffraction methods. The results are summarized as follows. In region I, there exist two critical micelle concentrations (CMC), indicating that this region is in a monomer – micelle equilibrium and that variation in the aggregated state occurs at the second CMC. Region II is a two phase area in which regions I and IV coexist. In region III, hydrated crystals and an aqueous solution of DPP coexist. Region IV is a homogeneous, transparent and fluid phase and the results of ^{31}P NMR spectra and x-ray diffraction patterns reveal the formation of a highly organized structure, similar to a lamellar-like structure. Region V is a homogeneous, transparent and fluid phase and the self-diffusion coefficient value and ^{31}P NMR spectra show that its phase structure is very similar to that for the concentrated sample in region I.

Key words Sodium di-*n*-pentyl phosphate – phase diagram – phase structure

Introduction

In many thermoanalytical studies [1–8] on the binary systems of water and phosphatidylcholine, it has been pointed out that water molecules incorporated into the polar layer of the aggregate systems play an essential role for the mechanism of the phase transition. Kodama et al. [9, 10] have demonstrated the predominant role of so-called "newly incorporated water" for phase change in dipalmitoylphosphatidylchorlne-water system in a detailed thermoanalytical study. For the same binary system, confirmational studies by the use of x-ray diffraction and infrared spectorscopic methods have also indicated that the water content plays an important role in the thermodynamic stable phase [11–13]. However, a phosphatidylcholine molecule is large in the size, and, moreover, has three kinds of polar groups (ester groups, and the phosphate anion and trimethylammonium cation moieties). Therefore, it is very difficult to discuss the interactions between each polar group and water molecules from the thermoanalytical data. It was thought that further understanding of the interactions between a phospholipid and water molecules would be obtained by using a simple surfactant molecule as a model of the phospholipid.

Dialkylphosphates with simple *n*-alkylchains are well suited for further investigation of a phospholipid. Thus far, the conformations of simple dialkylphosphate anions in aqueous solution have been studied mainly by infrared and Raman spectroscopic methods [14]. The x-ray crystallographic analysis of barium diethyl phosphate [15] showed that the two C–O bonds occupy gauche positions

with respect to the P–O bonds, confirming the conclusion of the spectroscopic studies.

In our previous paper [16], detailed Raman studies of the barium dipentyl phosphate-water system indicated that two types of aggregation structure with different $Ba^{2+} \cdots PO_4^-$ interaction modes coexist in the liquid crystal. Furthermore, it was found that the all-*trans* form of the alkyl group was favored in the micellar state. Recently, for the dipentylphosphate-water system [17], we demonstrated that the phase transition from the lyotropic state to the coagel phase leads to a marked variation in the conformation about the phosphodiester P–O bonds, and that this is strongly dependent upon the water content in the system. Although studies on simple dialkylphosphates have increased understanding of the physico-chemical properties of phospholipid aggregates, investigations of phase diagrams and phase structures of the simple dialkylphosphate-water binary systems are few in number.

We report the phase diagram of the sodium di-*n*-pentylphosphate-water system and discuss the phase structure in detail, using ^{1}H-pulsed-gradient NMR self-diffusion, ^{31}P NMR and x-ray diffraction studies.

Experimental

Materials

Sodium di-*n*-pentyl phosphate (DPP) was prepared as follows. Di-*n*-pentyl phosphochloridate, $(CH_3(CH_2)_4O)_2P(O)Cl$, was synthesized from phosphoryl chloride and 1-pentanol, using a method similar to that of Saunders et al. [18]. The fraction of bp 120° C/4 mmHg was collected. Di-*n*-pentyl phosphochloridate was treated with water, and the resulting HCl was pumped off to yield phosphoric acid di-*n*-pentyl ester, $(CH_3(CH_2)_4O)_2P(O)OH$. The ester was neutralized with a solution of NaOH and DPP was identified by ^{13}C NMR spectral and elemental analyses. Since the sodium salt was hygroscopic, the barium salt was used for the elemental analysis. Anal. $C_{20}H_{44}O_8P_2Ba$: Calcd: C, 39.26; H, 7.25. Found: C, 39.06; H 7.47.

Phase diagram determinations and calorimetry

Sample solutions were prepared by weighing the DPP and H_2O components into glass ampoules, which were then sealed and the contents homogenized by annealing. The thermotropic transition temperature of the DPP-water system was determined with a differential scanning calorimeter (Rigaku DSC 8230) which was scanned at a rate of 2° C/min by using a volatile pan with α-Al_2O_3 in the reference pan. The temperature dependence of the phase feature of the samples was determined by visual inspection as the ampoules were held in a temperature-controlled water-bath (rate of temperature elevation and cooling 0.1° C/min). The temperature was measured with a digital thermometer (Sato Keiryoki).

^{31}P NMR measurements

^{31}P NMR spectra were measured using high-power proton decoupling at 80.995 MHz on a Varian XL-200 spectrometer. The ^{31}P chemical shift (σ) of the DPP anions in D_2O solution were measured relative to the ^{31}P signal of aqueous 85%-H_3PO_4 solution.

Self-diffusion coefficient measurements

The Fourier-transform ^{1}H pulsed gradient (^{1}H FT-PG) NMR self-diffusion was measured on a JEOL FX-100 NMR Fourier Transform spectrometer, equipped with a gradient unit at 99.60 (^{1}H) MHz using an internal D_2O lock [19–22]. The absolute magnitude of the field gradient G was calibrated against the self-diffusion coefficient value (2.30×10^{-9} m^2 s^{-1}) of pure water (H_2O) at 25° C [23]. The temperature of the sample in the tube was measured with a thermocouple and was controlled to $\pm$ 0.5° C. The self-diffusion coefficients of DPP in D_2O were obtained from the $(CH_2)_4$- proton NMR signal of the pentyl-chain. For the two-phase solution in region II, measurements were made at the same controlled temperature immediately after separation of the upper and lower-layers.

x-ray diffraction measurements

x-ray diffraction low-angle patterns were obtained using a RU-200 camera (Rigaku Denki Co.) with a three slits-system in the diffraction range of $1.2° < 2\theta < 20°$. Nickel-filtered CuKα radiation ($\lambda = 1.54$ Å) was used. The temperature of the sample was controlled by air within $\pm$ 1° C and was measured with a digital thermometer (Sato Keiryoki).

Results and discussion

Phase diagram of the DPP-water system

Figure 1 shows the phase diagram of the DPP-water system, which consists of five regions. For the representative sample solutions of the concentrated DPP-water system, the phase-transition temperatures and the ΔH values

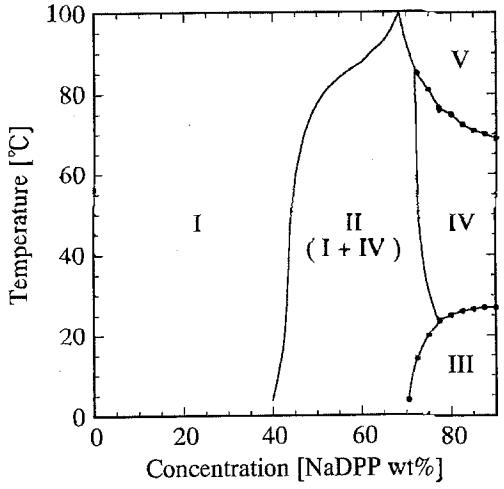

Fig. 1 Phase diagram of DPP-water system: A (100° C, 68.5 wt %), B (85.0° C, 72.5 wt %) and C (23.2° C, 77.3 wt %). Region I: homogeneous aqueous solution; region II: two-phase solution; region III: solid DPP and its solution; region IV: homogeneous and transparent gel; region V: transparent and liquid solution. Solid lines shows the phase boundary lines assumed by the visual inspection, and solid circles indicate the phase transition points determined by DSC curves

obtained from DSC curves are listed in Table 1. A homogeneous and transparent one-phase solution was obtained in region I, while region II is a two-phase solution system, having transparent upper and lower layers. For region II, it was found that the volume percentage of the upper layer decreased linearly and, conversely, that of the lower layer increased with an increase in weight-percentage of DPP. This observation is a consequence of the lever rule and proves that the two-phase system is in equilibrium in region II. In region III, hydrated crystals and an aqueous solution DPP were found to coexist. For region IV, a homogeneous, transparent and viscous one-phase solution was obtained at higher temperatures, and could be regarded as a gel phase at room temperature. In region V, a homogeneous, transparent and fluid phase was obtained. The optically-isotropic properties of samples in the lower layer of region II and in region IV were confirmed under a polarizing microscope.

Self-diffusion coefficients and aggregate structure

Self-diffusion coefficients provide important information on aggregate structure and association behavior, because molecular association in solution greatly affects the translational motion of a molecule. It has been suggested that measurement of self-diffusion coefficients is a direct approach for elucidating the structural organization of aggregated systems [23].

Table 1 The phase transition temperatures (T_t, °C) and the ΔH (J g^{-1}) values

wt %	T_t	ΔH
60.00	81.8	6.74
70.04	3.9	8.49
	95.5	11.17
79.86	24.7	73.68
	74.8	2.93

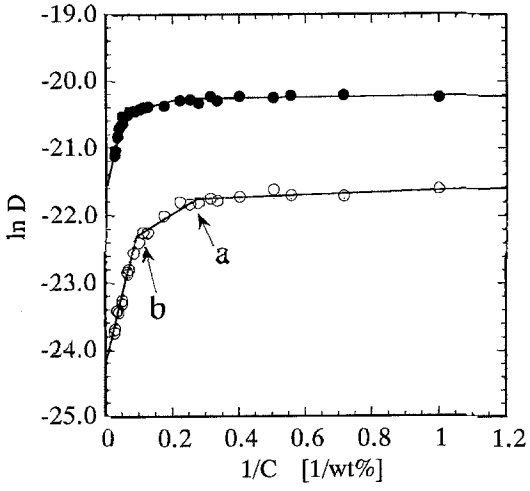

Fig. 2 The ln$D$ vs. 1/C plots for the DPP-D_2O system in region I. a: 4.7 wt % and b: 10.7 wt % Filled circle (●) and open circle (○) correspond to the results of water and DPP anions, respectively

The self-diffusion coefficients (D) of the DPP anions in water were measured for regions I, IV and V. Figure 2 shows the ln D vs. inverse concentrations (1/C) plots for region I at 25° C. In the plots, two inflection points are found at concentrations of 4.7 and 10.7 wt%. Below a concentration of 4.7 wt %, the D values are almost constant ($(4.09 \sim 4.14) \times 10^{-10}$ m^2 s^{-1}), but above this concentration they tend to decrease with an increase in concentration. This observation can be explained by a simple two-site model [24], which is in a single monomer $\Leftrightarrow$ micelle equilibrium state. In this model, the DPP-water system contains a finite concentration of the DPP anion monomer, contributing to the observed self-diffusion coefficient. The observed self-diffusion coefficients are population-weighted averages of the D value of the monomer and that of the micelles, and are given by Eq. (1),

$$D = PD_{\text{mic}} + (1 - P)D_{\text{mono}} \quad (1)$$

where $P = (C - \text{CMC})/C$, C is the total concentration of DPP, and D_{mono} and D_{mic} are the self-diffusion coefficients of the DPP anions in the monomer and micellar states,

Table 2 Self-diffusion coefficients (D, 10^{-10}[$m^2 s^{-1}$]) and activation energies (E_a, kJ mol^{-1})

	wt %	D				E_a
		25° C	50° C	70° C	80° C	
Phase I	3.8	4.08 ± 0.27	6.65 ± 0.22	–	–	20.3 ± 1.2
	15.0	1.17 ± 0.02	2.40 ± 0.33	–	–	26.7 ± 0.9
	30.0	0.49 ± 0.01	1.43 ± 0.05	–	–	32.0 ± 2.5
	34.9	0.51 ± 0.01	1.15 ± 0.09	–	–	35.4 ± 1.6
Phase IV	75.0	–	–	0.53 ± 0.02	–	67.0 ± 3.6
Phase V	75.0	–	–	–	0.91 ± 0.26	36.0 ± 0.8

respectively. Thus, the first inflection point should be due to formation of micelles.

The variation of the ln$D$ at the first CMC (4.7 wt %) is not so marked. However, as discussed later, the existence of the first CMC (4.6 wt %) was confirmed by the concentration dependence of the ^{31}P NMR chemical shift.

As the concentration increases beyond the first CMC, the D value tends to decrease. However, the slope in the plots changes markedly at concentrations greater than 10.7 wt %, which can be regarded as a second CMC. It has already been reported for surfactant solutions that the micellar structure changes above the second CMC [24]. Therefore, we may assume for simple dialkyl phosphate anions that such a variation in the aggregate state occurs above the second CMC.

For the two-phase solution in region II, self-diffusion measurements at the same controlled temperature were made immediately after separation of the upper and lower layers. We have confirmed that there is a marked difference in the D values of the upper and lower layers and that the D values of the upper layer are very close to those of region I while those of the lower one are similar to those of region IV. Thus, in region II we may assume that regions I and IV coexist and that the two phases are in equilibrium. This conclusion is also supported by ^{31}P NMR results.

The D values of water molecules are constant below the first CMC, while beyond this concentration the values tend to decrease slightly until they rapidly decrease above the second CMC. Such a behavior for the D value of water molecules at concentrations above the first CMC comes from the increased contribution of the slow motion of hydrated water molecules, and the obstruction effect of micellar formation.

The activation energy (E_a) for the self-diffusion of the DPP anions has been measured for regions I, IV and V, as listed in Table 2. The size of the micelle and the viscosity of the solvent which depends exponentially on the temperature, contribute to the D value. Therefore, the observed E_a value reflects the macroscopic behavior of a phase. The E_a value (20.3 kJ mol^{-1}) obtained at a concentration of 3.8 wt % obviously reflects self-diffusion of the mono-dispersed DPP anions. The activation energy (E_a = 26.7 kJ mol^{-1}), which has been determined for the 15 wt % DPP solution, should be regarded as a superposition of contributions from the fast diffusion of mono-dispersed DPP anions and the slow diffusion of the micelles. The E_a values of 32.0 ~ 35.4 kJ mol^{-1}, obtained for the samples at concentrations above the second CMC, imply a restricted state for DPP anion diffusion in this region.

Figure 3 shows the temperature dependence of the self-diffusion coefficient for the 75 wt % DPP solution. the ln$D$ vs $1/T$ plot consists of two straight lines, the temperature (348K) at the inflection point corresponds to the transition temperature from region IV to region V in the DPP-D_2O system. Activation energies obtained for the two regions are listed in Table 2. The high activation energy (67.3 ± 3.58 kJ mol^{-1}) for region IV indicates that the DPP anions are in an extremely restricted state. In region V, the D value at higher temperatures is very close to that of the DPP anions in the concentrated samples in region I, thereby indicating a similarity in their aggregated structure.

^{31}P NMR chemical shifts and ^{31}P signal shapes

Only narrow and symmetrical ^{31}P resonance signals were observed for region I, reflecting an isotropic motional averaging of monomers and Brownian tumbling of the DPP micelles. The ^{31}P chemical shift (σ) vs. log($1/C$) plot is shown in Fig. 4. Two inflection points are observed, at concentrations of 4.6 and 17.0 wt %. Such a concentration dependence of the ^{31}P σ values can also be explained by a pseudo-phase and two-site model. The observed chemical shift (σ) is a weighted average of the chemical shifts in a monomeric and micellar states, since the exchange rate of the DPP anions between the bulk solution and the micelles is very fast. Thus, the observed σ value is expressed [24] by Eq. (2),

$$\sigma = (\mathrm{CMC}/C)\sigma_{\mathrm{mono}} + [(C - \mathrm{CMC})/C]\sigma_{\mathrm{mic}} \quad (2)$$

(assuming that the concentration in the monomeric state is constant above the CMC), where C is the total concentration of DPP, and σ_{mono} and σ_{mic} are the ^{31}P chemical shifts

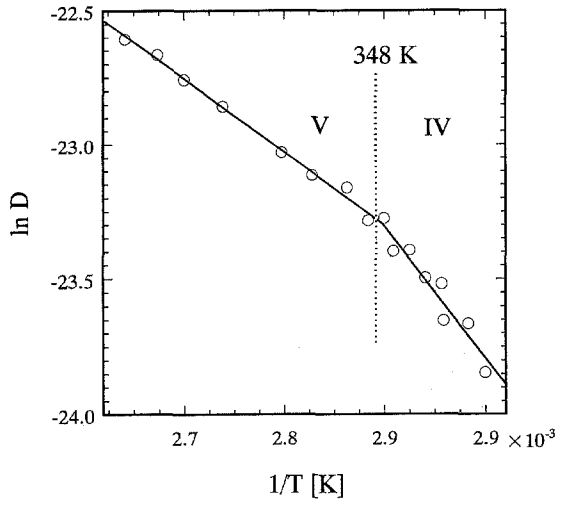

Fig. 3 Temperature dependence of the D-value for the 75 wt %-DPP solution

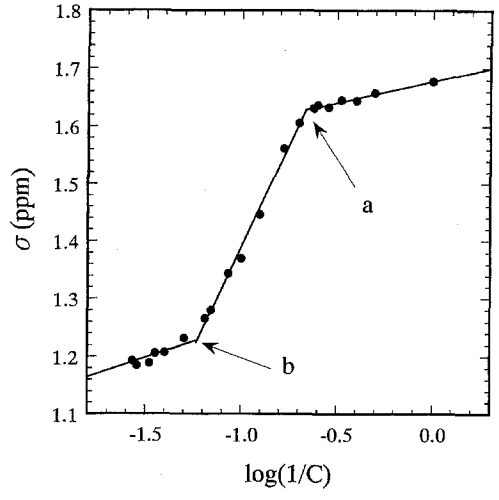

Fig. 4 ^{31}P chemical shift (σ) vs. log(1/C) plots for region I: a: 4.6 wt %, b: 17.2 wt %

for the monomers and micelles, respectively. Plots of σ vs. log(1/C) are well described by Eq. (2). The first inflection point (4.6 wt %), therefore, implies the presence of a CMC and gives a value in good agreement with that (4.7 wt %) obtained from the plot of ln$D$ vs 1/C.

For region I, in the concentrated region, there is another inflection point at a concentration of 17.1 wt %, which may then be regarded as the second CMC, although this value is greater than that (10.7 wt%) obtained from the plot of ln D vs. 1/C.

Variation of the D value at the CMC is a direct reflection of the association behavior of the hydrocarbon part of a DPP anion, since the resonance signals of methylene-protons were used for measurements of the D value. However, variation of ^{31}P σ may be caused by shielding effect of Na^+ counter ion to PO_4^- anion. The extent of screening of the counter ion is strongly dependent on the aggregate structure, as discussed later. In fact, the degree of ionization (α), obtained by small angle neutron scattering analysis (to be published separately), is 0.3 at a concentration of 10 wt %. Therefore, for highly concentrated solutions in region I, it may be assumed that the degree of ionization at the interface of aggregates becomes very small. Thus, the second CMC, obtained from the concentration dependence of the ^{31}P σ value, may reflect variation of the polar electrical-double layer structure, due to the structural change in the DPP micellar aggregate. Furthermore, the x-ray diffraction patterns provide evidence that a lamellar-like structure may be present in concentrated solutions in region I, as discussed below. We may assume that polar groups are more densely packed in a lamellar-like structure than in a micelle, since the increased screening action of counter ions results in a decrease in the repulsive force between the anions.

Thus, at the second CMC, variation of the aggregate structure may cause an environmental change to polar layer, resulting in a difference between the second CMC values determined by measurements of the ^{31}P σ and D values.

It has already been found for dihexanoylphosphatidylcholine [25] that micellization brings about a shift of the ^{31}P NMR signal and that the ^{31}P σ vs. log(1/C) plots could be explained by Eq. (2). Matshushita et al. [26] and Yoshida et al. [27] have also reported that, for the simple mono- and di-alkylphosphate-water systems, an upfield shift of the ^{31}P signal (caused by micellization) is caused by complex formation between the phosphate anions and the counter ions [28, 29]. Therefore, the upfield shift of the ^{31}P signal seen for DPP anions may be explained by formation of such a complex.

For the samples in region I, it has been found that the half-height width ($\Delta\nu^{1/2}$) of the ^{31}P signal depends upon the concentration of DPP (data not shown). The $\Delta\nu^{1/2}$ results may be summarized as follows. The $\Delta\nu^{1/2}$ values (0.023 ppm) are almost constant below the first CMC, and are almost equal to that (0.025 ppm) of diethylphosphate anions in the monomeric state, reflecting an isotropic motion of the whole molecule. The $\Delta\nu^{1/2}$ value observed at concentrations between the first and second CMCs is also a weighted average of the $\Delta\nu^{1/2}$ values for the monomers and micelles in the two-site model [23]. The $\Delta\nu^{1/2}$ value increases with an increase in concentration above the first CMC, and a further increase of the half-height width occurs at concentrations above the second CMC.

For region II, the ^{31}P NMR spectra of the upper and lower layers were also measured. For the upper layer, only

a symmetrical ^{31}P signal having a narrow half-height width was observed, and the σ and $\Delta\nu^{1/2}$ values are very similar to those for the micellar solutions in region I. Therefore, for the upper layer, the ^{31}P signal comes from the micelles which are in equilibrium with the monomers. Conversely, for the lower layer in region II, an asymmetric ^{31}P signal having a low-field shoulder similar to that for the sample in region IV appears (Fig. 5), showing that the ^{31}P signal for the lower layer arises from the ordered aggregate system. The characteristic asymmetry for the ^{31}P signal should be due to the chemical shift anisotropy ($\Delta\sigma = \sigma_\perp - \sigma_\parallel$) of a ^{31}P nucleus in the phosphate group, arising from restricted anisotropic motion of the DPP anions. Thus, the results of the ^{31}P NMR spectra support the coexistence of regions I and IV in region II.

For region IV, we have confirmed that the ^{31}P NMR spectra also provide the asymmetric ^{31}P signal in which the $\Delta\sigma$ value strongly depends upon the temperature, as shown in Fig. 5. An increase in temperature brings about a marked chemical shift anisotropy for the ^{31}P signals, indicating that a highly-organized structure of phosphate anions is formed. The ^{31}P line shape suggests that formation of a lamellar-like structure occurs in this region, as confirmed by x-ray diffraction (to be published separately). In particular, for the sample solution in region IV, the ^{31}P chemical shift anisotropy ($\Delta\sigma$) tends to increase with an increase in temperature. This observation is typical of an alignment of ^{31}P chemical shift tensors perpendicular to the magnetic field with a narrow angular distribution about the direction of the magnetic field. In fact, for the dibutylphosphate-water system [30], this orientation effect has been found to be characteristic of DM II type-discotic lyomesophase [31], formed, by aggregation of large dislike micelles in the magnetic field.

Thus, we can assume that the lower layer in region II and region IV are more structurally organized compared with region I and the upper layer in region II.

For region V, symmetric and narrow ^{31}P NMR signals have been observed, indicating that this region is the isotropic phase.

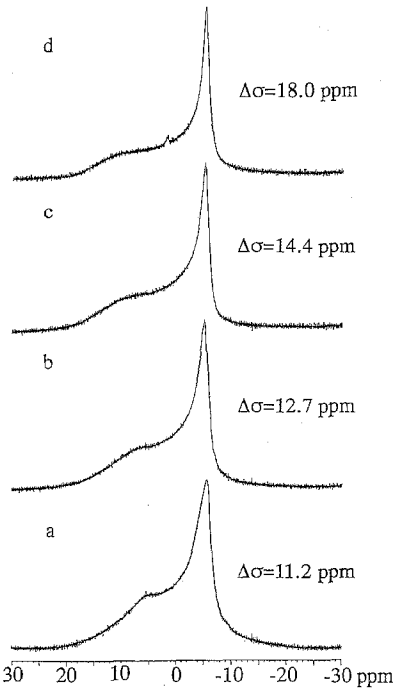

Fig. 5 ^{31}P NMR spectra of the samples in region IV at various temperatures (a: 25° C, b: 50° C, c: 70° C and d: 90° C) and the chemical shift anisotropies ($\Delta\sigma = \sigma_\perp - \sigma_\parallel$)

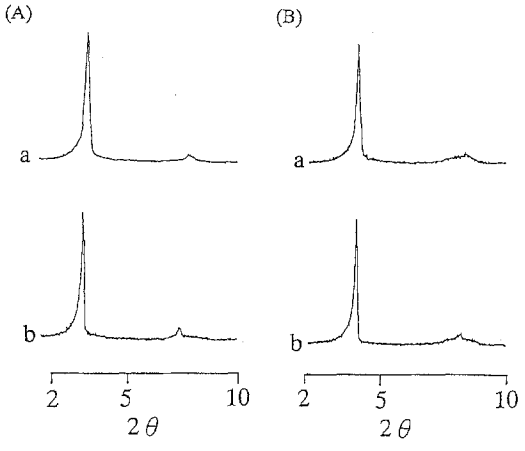

Fig. 6 x-ray diffraction patterns of the DPP-water system at 25° C (a) and 90° C (b) : (A) lower-layer sample (50 wt %, region II), (B) 72 wt % (region IV)

x-ray diffraction pattern

The x-ray low-angle diffraction patterns of the samples were measured at different temperatures, to aid further understanding of the phase for the DPP water system. Figure 6 shows the x-ray diffraction patterns of the DPP-H_2O systems. For the lower layer samples in region II and the samples in region IV, the lattice spacings at 18.8 and 26.9 Å are observed within the temperature range 25 ~ 90°C. The strong reflection at 3 ~ 5° corresponds to the first-order reflection and the very weak reflection at 8.3° to the second-order reflection. This observation indicates that an ordered structure of DPP aggregates is formed in these phases.

The corresponding interplanar spacings (**d**) for the DPP-H_2O systems are listed in Table 3 and show that the **d** values are strongly dependent upon concentration. However, the effect of temperature is very small, implying that

Colloid & Polymer Science, Vol. 273, No. 11 (1995)

Table 3 The interplanar spacings d[Å] and the r[Å] values*

wt %	25° C		50° C		70° C		80° C		90° C	
	d	*r*	*d*	*r*	*d*	*r*	*d*	*r*	*d*	*r*
80	19.5	26.8	19.7	24.5	18.8	24.7	18.8	24.4	19.3	24.4
76	26.0	26.9	25.9	24.6	26.3	24.9	26.7	24.5	20.3	24.7
72	21.5	26.6	20.6	25.6	20.4	25.5	20.4	25.6	20.8	25.6
65	22.5	26.0	21.1	25.9	21.4	25.6	20.6	25.3	21.5	25.9
50	23.0	28.1	22.5	26.9	22.6	26.9	20.7	26.3	21.9	27.2

*The separation between two high electron density peaks in the radial distribution function calculated by Fourier transformation

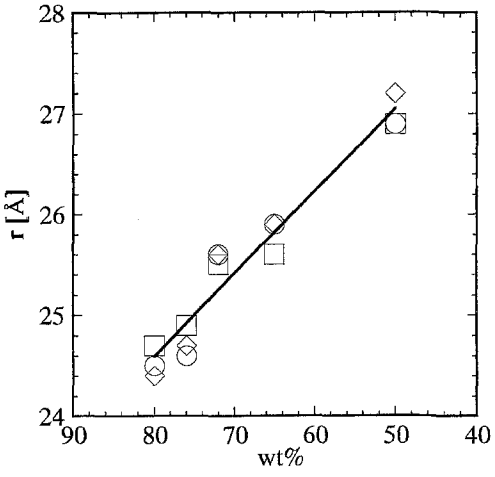

Fig. 7 Concentration dependence of the **r** values for the DPP-water system at different temperatures: (△) 50° C, (□) 70° C and (○) 90° C

the ordered structure of the DPP aggregates is very stable in the temperature range 25 ~ 90°C.

Since the ^{31}P NMR spectra for the lower layer samples in region II and those in region IV show asymmetric characteristics of a bilayer-type structure with respect to their line shapes, the observed **d** values possibly reflect the concentration-dependence of the thickness of a bilayer.

The radial electron density distributions were calculated by Fourier transformation of the x-ray diffraction intentisites. The separation (**r**, Å) between two high electron density peaks may be useful as a measure of the distance between two polar-layers sandwiched between the hydrocarbon layers. The dependence of the **r** value on concentration is shown in Fig. 7. The **r** values are 27 Å at high water-content and 24.5 Å at low-water content. In particular, the **r** values (24 ~ 25 Å) obtained from the concentrated samples correspond closely to the thickness of a bilayer whose formation can be assumed from the geometrical structural parameters of the DPP molecule. Thus, the x-ray diffraction data provide further evidence for the ordered structure of the aggregate system which was assumed from the self-diffusion and ^{31}P NMR behavior.

Conclusion

The phase diagram and phase structure of the DPP-water system have been investigated by ^{1}H pulsed-gradient NMR self-diffusion, ^{31}P NMR, and x-ray diffraction methods. The results can be summarized as follows.

1. The phase diagram of the DPP-water system consists of five regions (I, II, III, IV and V). Region I is a homogeneous and transparent one-phase solution and region II a two-phase solution having transparent upper and lower layers. In region III, hydrated crystals and a solution of DPP coexist. Region IV is a transparent gel phase at room temperature and a homogeneous, transparent and viscous one-phase solution at higher temperature. Region V is a homogeneous, transparent and fluid phase.

2. For region I, the presence of first and second values of the CMCs can be assumed from the results of the self-diffusion coefficient and ^{31}P NMR spectra. The first CMC values (4.6 and 4.7 wt %) obtained by the two methods are in good agreement each other. However, for the second CMC, the value (17.1 wt %) obtained by ^{31}P NMR is greater than that (10.7 wt %) determined by a plot of ln D vs. $1/C$. The marked difference between these second CMC values arises from the different methods of determination: the ^{31}P NMR method reflects environmental variation of the polar layer and, in particular, the binding process of the counter ions. while the D value method depends upon the translational motion of a hydrocarbon tail. Region II is a two-phase area in which regions I and IV coexist. However, for region IV and DPP anions are in an extremely restricted state and the highly-organized structure of the phosphate anions is formed. Moreover, the D value and ^{31}P NMR show that region V is isotropic and its plane structure is very similar to that for the concentrated sample in region I.

3. The radial electron density distributions indicate that a highly-organized structure is formed for the concentrated samples in region I, for the lower layer sample in region II, and in region IV, and that the structure is similar

to that of a bilayer having a thickness which depends on the concentration. The results of the low-angle x-ray diffraction patterns for the highly-organized structure agree well with those qualitatively predicted by ^{31}P NMR spectra.

Acknowledgement We express gratitude to Prof. Chairman J. O'Conner (University of Auckland, Department of Chemistry, New Zealand) and Dr. Tadashi Kato (Department of Chemistry, Tokyo Metropolitan University, Japan) for reading the manuscript prior to publication and making suggestions for its revision.

References

1. Chapman D, Williams RM, Ladbrooke BD (1967) Chem Phys Lipids 1:445–474
2. Hing HJ, Sturtevant JM (1972) J Biol Chem 247:6071–6075
3. Salsbury NJ, Darke A, Chapman D (1972) Chem Phys Lipids 8:142–151
4. Tardieu A, Luzzati V, Reman FC (1973) Mol Biol 75:711–733
5. Janiak MJ, Small DM, Shipley GG (1976) Biochem 15:4575–4580
6. Inoko Y, Mitsui T (1978) J Phys Soc Jap 44:1918–1924
7. Doniach S (1979) J Chem Phys 70: 4587–4596
8. Inoko Y, Mitsui T, Ohki K, Sekiya T, Nozawa Y (1980) Phys Stat Sol (a) 61:115–121
9. Kodama M, Tsujii K, Seki S (1990) J Phys Chem 94:815–819
10. Kodama M, Hashigami H, Seki S (1987) J Colloid Interface Sci 117:497–504
11. Füldner HH (1981) Biochem 20: 5707–5710
12. Ruoccp MJ, Shipley GG (1982) Biochem Biophys Acta 684:59–66
13. Cameron DG, Mantsch HH (1982) Biophys J 38:175–184
14. Shimanouchi T, Tsuboi M, Kyogoku Y (1964) Adv Chem Phys 7:435–498
15. Kyogoku Y, Iitaka Y (1966) Acta Crystallogr 21:49–57
16. Okabayashi H, Yoshida T, Ikeda T, Matsuura H, Kitagawa T (1982) J Amer Chem Soc 104:5399–5402
17. Okabayashi H, Taga K, Miyagai K, Uehara T, Yoshida T, Nishio E (1991) J Phys Chem 95:7932–7938
18. Saunders BC, Stacey GJ, Wild F, Wilding IGE (1948) J Chem Soc:699–703
19. James TL, McDonald GG (1973) J Magn Reson 11:58–61
20. Stejskal EO, Tanner JE (1965) J Chem Phys 42:288–292
21. Hahn EL (1950) Phys Rev 80:580–594
22. Kato T, Seimiya T (1986) J Phys Chem 90:3159–3167
23. Persson B-O, Drakenberg T, Lindman B (1979) J Phys Chem 83:3011–3015
24. Wennerstrom H, Lindman B, Söderman O, Drakenberg T, Rosenholm JB (1979) J Amer Chem Soc 101:6860–6864
25. Roberts MF, Adamich M, Robson R-J, Dennis EA (1979) Biochem 15:3301–3308
26. Matsushita K, Kamo O, Terada Y, Yoshida T, Okabayashi H (1984) Chem Scripta 23:228–232
27. Yoshida T, Miyagai K, Taga K, Okabayashi H, Matsushita K (1990) Magn Reson in Chem 28:715–721
28. Crutchfield MM, Callis CF, Irani RR, Roth GC (1962) Inorg Chem 1:389–393
29. Jardetsky O, Werts JE (1960) J Amer Chem Soc 82:318–323
30. Chachaty C, Quaegebeur (1983) J Phys Chem 87:4341–4343
31. Forrest BJ, Reeves LW (1981) Chem Rev 81:1–14